Available online at www.sciencedirect.com
SCIENCE DIRECT®
ELSEVIER
International Journal of Multiphase Flow 31 (2005) 371–392
International Journal of Multiphase Flow
www.elsevier.com/locate/ijmulflow

Explosive boiling of water in parallel micro-channels

G. Hetsroni *, A. Mosyak, E. Pogrebnyak, Z. Segal

Department of Mechanical Engineering, Technion—Israel Institute of Technology, Haifa 32000, Israel

Received 23 September 2004; received in revised form 3 January 2005

Abstract

The objective of this study is to visualize the flow pattern and to measure heat transfer coefficient during explosive boiling of water in parallel triangular micro-channels. Tests were performed in the range of inlet Reynolds number 25–60, mass flux 95–340 kg/m^{2}s, and heat flux 80–330 kW/m^2.

The flow visualization showed that the behavior of long vapor bubbles, occurring in a micro-channel at low Reynolds numbers, was not similar to annular flow with interposed intermitted slugs of liquid between two long vapor trains. This process may be regarded as explosive boiling with periodic wetting and dryout.

In the presence of two-phase liquid–vapor flow in the micro-channel, there are pressure drop oscillations, which increase with increasing vapor quality.

This study shows strong dependence of the heat transfer coefficient on the vapor quality. The time when liquid wets the heated surface decreases with increasing heat flux. Dryout occurs immediately after venting of the elongated bubble.

Keywords: Micro-channel; Flow boiling; Heat transfer; Two-phase flow pattern; Dryout

1. Introduction

Boiling in heated micro-channels is of significant importance for many applications, in particular, for cooling systems of electronic devices. There is a scale effect which becomes evident when

* Corresponding author. Tel.: +972 48 292058; fax: +972 48 238101.
E-mail address: hetsroni@techunix.technion.ac.il (G. Hetsroni).

0301-9322/$ - see front matter © 2005 Published by Elsevier Ltd.
doi:10.1016/j.ijmultiphaseflow.2005.01.003

the hydraulic diameter is less than the capillary length $[\sigma/g(\rho_L - \rho_G)]^{0.5}$, where σ is the surface tension, ρ_L and ρ_G is the liquid and the vapor density, respectively. In the present study, the hydraulic diameter of the channels ($d_h = 129$ μm) was smaller than the capillary length.

Jiang et al. (2001) performed visualization and measurements of flow boiling in silicon micro-channels of triangular cross-sections of $d_h = 26$ and 53 μm. They did not observe bubbly flow in the micro-channels. Periodic wetting and rewetting phenomena were observed by Hetsroni et al. (2001, 2002, 2003a,b), Zhang et al. (2002), Steinke and Kandlikar (2003) and Kandlikar and Balasubramanian (2004). Hetsroni et al. (2001, 2003a,b) investigated flow boiling of water in silicon triangular parallel micro-channels of $d_h = 103$, 129 and 161 μm. The bubble growth and temporal variation of bubble size were studied. Explosive vaporization and significant pressure drop fluctuations were observed. Flow patterns, observed in these studies and reported also by Kandlikar (2002), revealed flow reversal in some channels with expanding bubbles pushing the liquid–vapor interface both upstream and downstream. It was reported by Hetsroni et al. (2002) that fluctuations of saturation temperature correspond to that of the pressure.

Zhang et al. (2002) carried out an experiment on flow boiling in silicon rectangular micro-channels of $d_h = 25$–60 μm. They found that boiling occurred with less than 5 K of superheat and they observed mostly annular flow with a very thin layer of liquid. However, the bubbly and slug flows typically observed in the macro-channels were absent from their experiment. Serizawa et al. (2002) studied flow pattern in air–water flow in circular tubes of 20, 25, and 100 μm and steam-water flow in a 50 μm circular tube. It has been confirmed that two-phase flow patterns are sensitive to the surface conditions of the inner wall of the test tube. Dry and wet areas were observed at low vapor velocities. Flow boiling of water, in parallel silicon micro-channels having trapezoidal cross-sectional area with hydraulic diameters of 158.8 and 82.8 μm, was studied by Wu and Cheng (2003, 2004). Long period fluctuations in fluid pressure, fluid temperature, and fluid mass flux were measured.

Mehendale et al. (2000) and Kandlikar (2002, 2004) recently presented an extensive review of single-phase and two-phase micro-channel heat transfer. Qu and Mudawar (2003) presented and discussed experimental results, which provide physical insight into the unique nature of saturated flow boiling heat transfer in a water-cooled micro-channel heat sink. The micro-channel heat sink contained 21 parallel channels having a 231×713 μm cross-section. The inlet Reynolds number ranged from 60 to 300. Contrary to macro-channel behavior, the heat transfer coefficient was shown to decrease with increasing thermodynamic equilibrium quality. This unique trend was attributed to appreciable droplet entrainment and onset of the annular flow regime. Such trend of heat transfer coefficient with quality was also reported by Hetsroni et al. (2002) for a heat sink that had 21 parallel triangular micro-channels of $d_h = 129$ μm. Vertrel XF (with a saturation temperature of 52 °C) was used as the working fluid in this study. Steinke and Kandlikar (2003) studied flow boiling of water in six parallel micro-channels. The average channel dimensions were 214 μm wide by 200 μm deep and 57.15 mm long. The local heat transfer coefficient decreased as the local quality increased. Yen et al. (2003) investigated convective boiling of HCFC 123 and FC 72 in a single tube. The inner diameters were 0.19, 0.3 and 0.51 mm, the working fluid was heated and its temperature was at 10 K below the saturated temperature. They showed that in the saturated boiling regime, the heat transfer characteristics were much different from those in conventional-size tubes. The heat transfer coefficient monotonically decreased with increasing vapor quality.

Flow boiling correlations for large diameter tubes developed by Kandlikar (1990) were modified for flow boiling in; what they referred to as; mini-channels and micro-channels. The correla-

tions were extended to laminar flow in micro-channels at $Re < 100$ and compared to the experimental data of Yen et al. (2003) for single tubes of diameter 0.19 mm. Based on the data set investigated using the proposed correlation, it was concluded that boiling was dominated by nucleation processes for low Reynolds numbers ($Re < 100$) in micro-channels. The correlations proposed were verified for refrigerants as coolant in the range of Reynolds number $Re = 72$–1490, but they were not verified for water flow. Liquid film formation was proposed as a key parameter that affects heat transfer coefficient in the models of saturated boiling in micro-channels.

Moriyama and Inoue (1996) performed experiments to measure the thickness of the liquid film formed by a growing flattened bubble in a narrow gap whose width ranged from 0.1 to 0.4 mm. A narrower gap caused faster growth of the bubble. The film thickness was about 2–7 μm depending on the gap size and initial superheat. Ory et al. (2000) solved numerically the growth and venting of a vapor bubble in a tube with a diameter of 62.5 μm and a length of 2 mm. The tube was open at both ends and connected two liquid reservoirs at constant pressure. This model simulated the effect of an intense, localized, brief heating of the liquid, which caused the nucleation and growth of a bubble.

An annular flow model was developed by Qu and Mudawar (2003a) to predict the saturated flow boiling heat transfer coefficient. Laminar liquid and vapor flow, smooth interface, and strong droplet entrainment and deposition effects were incorporated into the model. The experimental results of micro-channel flow boiling of water at $Re = 300$–600 obtained previously by Qu and Mudawar (2003b) were compared to this model. The model correctly captured the overall trend of decreasing heat transfer coefficient with increasing vapor quality in the low vapor quality region ($0 < x < 1$) of the micro-channels.

Thome et al. (2004) proposed a new heat transfer model for evaporation in the elongated-bubble regime in micro-channels. The model describes the transient variation in local heat transfer coefficient during the sequential and cyclic passage of a liquid slug, an evaporating elongated bubble and a vapor slug. The initial thickness of the liquid film is a key parameter in the model. For this purpose, the Moriyama and Inoue (1996) correlation was used. The main difficulty in implementation of the method of Moriyama and Inoue (1996) is in estimating the time for the front of the bubble to reach a particular radius. Thome et al. (2004) developed the expression for film thickness only from R-113 tests. The time averaged local heat transfer coefficient calculated using this model was compared by Dupont et al. (2004) to 1591 experimental data, for tube diameters from 0.77 to 3.1 mm. The data were obtained for the following seven fluids: R-11, R-12, R-113, R-123, R-134a, R-141b, and CO_2. The new model predicts 67% of the database to within ±30%.

Thome et al. (2004) assumed that at a fixed location, the process proceeds as follows: (i) a liquid slug passes, (ii) an elongated bubble passes, (iii) if the thin evaporating film of the bubble dries out before the arrival of the next liquid slug, then a vapor slug passes. The cycle then repeats itself upon arrival of the next liquid slug. Thus, the flow pattern is similar to video images of elongated bubble adiabatic air–water flow taken under consideration in the study of Thome et al. (2004). It was shown by Hetsroni et al. (2003a,b) that flow pattern in adiabatic air–water flow is quite different from that for evaporation in micro-channels. The data for comparison of the model to experimental results presented by Thome et al. (2004) were obtained for single channels whose inner diameters were considerably larger than those employed in micro-channel heat sinks. Heat transfer in a heat sink containing multiple parallel channels may be significantly different from that in a single channel.

The goal of the present study is to examine flow pattern and heat transfer in the saturated water flow boiling in parallel micro-channels at low Reynolds numbers. This paper is directed toward micro-channels, which consist of cooling channels in blocks, as opposed to single channels that are usually thermally well controlled. The channels used in the present study were etched in a block of silicon, with microelectronic fabrication techniques. Heat was supplied to one side of the block. Since the channels were etched in one side, a cover plate was provided on that side, and inlet and exit manifolds connected the test module to the flow system. Bubble dynamics in a micro-channel is quite different from that in an ordinary sized channel. Bubble growth in a micro-channel is restrained by the channel wall in the transversal direction. The two-phase flow pattern, observed simultaneously in the channels, may be different, depending on mass and heat fluxes. The flow distribution among parallel channels is a particularly serious concern with boiling flows. The shape of the channel, conjugate effects, circumferential and axial heat conduction in the material forming the channel affect the nucleation. The system studied is very complex, but is considered capable of obtaining significant features of explosive boiling in micro-channels.

2. Experimental set-up and procedure

2.1. Experimental facility

The experimental facility, Fig. 1, and flow loop were described in detail by Hetsroni et al. (2002, 2003a,b). The loop consists of a liquid peristaltic pump, piping, test module, entrance and exit

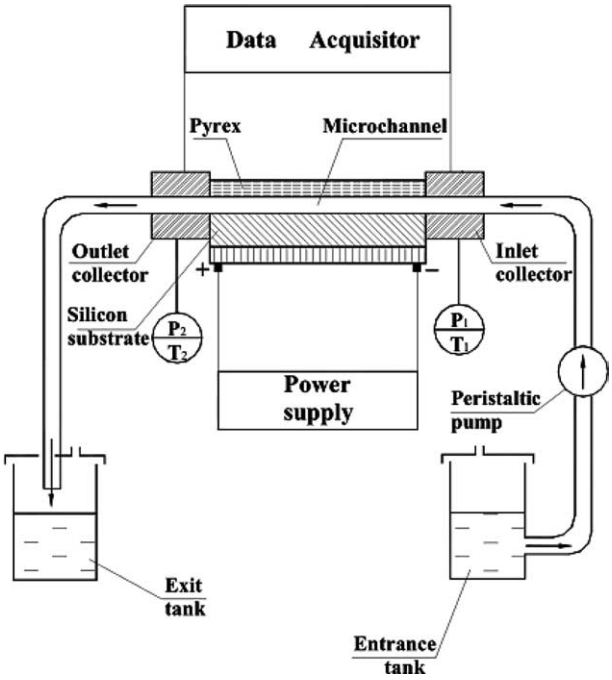

Fig. 1. Experimental facility.

tanks. Deionized (not degassed) water was used in this study. The desorption of the dissolved gases formed bubbles of gas and a limited amount of bubbles containing gas–water vapor mixture. As a result, boiling incipience occurred at channel wall temperature below that of saturation temperature. This result agrees with previous investigators works. Steinke and Kandlikar (2004) studied flow boiling in six parallel micro-channels, each having a hydraulic diameter of 207 μm. During the flow boiling studies with water in these micro-channels, nucleation was observed at a surface temperature of 90.5 °C for the dissolved oxygen content of 8.0 parts per million (ppm) at a pressure of 1 atm. As the surface temperature of the channel approached the saturation temperature, the effect of dissolved gases vanished. The effect of dissolved gases on boiling heat transfer of water was studied by McAdams et al. (1949). In the partial boiling region, the heat transfer coefficient increased due to increased nucleation activity. However, this effect completely disappeared at higher wall superheats as fully developed boiling conditions were established. This was well illustrated by Rohsenow et al. (1985). It was shown that there is no effect of dissolved gases in the fully developed boiling region between completely degassed water and water with a very high dissolved air component. Similar results were reported by Kandlikar and Bulut (2003). The results discussed in the present study were obtained when the channel wall temperature exceeded the saturation temperature. Working liquid was pumped from the entrance tank through the inlet collector to the micro-channels in the test module, and from the micro-channels through the outlet collector to the exit tank. Tubing of 4.0 mm inner diameter delivered the pumped fluid into the test module and out to the exit tank. The experiments were performed in an open loop, therefore the outlet pressure was close to atmospheric.

The temperature of the working fluid was measured at the inlet and outlet collectors of the test module, by 0.3 mm type-T thermocouples. The thermocouples were calibrated in 0.1 K increments. The flow rate of the working fluid was controlled by adjusting the frequency of the peristaltic pump and was measured by weighting method. Pressures were measured at the inlet and the outlet of the test module by silicon pressure sensors, with sensitivity of 3.3 mV/kPa, response time 1.0 ms. The data were collected by a data acquisition system.

2.2. Basic design of the test sections

The test module is shown in Fig. 2. It was fabricated of a square-shape silicon substrate 15×15 mm, 530 μm thick, and utilized a Pyrex cover, 500 μm thick, which served as both an insulator and a transparent cover through which flow in the micro-channels could be observed. The Pyrex cover was anodically bonded to the silicon chip, in order to seal the channels. In the silicon substrate, twenty one parallel micro-channels were etched the cross-section of each channel was an isosceles triangle with base $a = 250$ μm. The angles at the base were 55°. An electrical heater of 10×10 mm^2, made of a thin film resistor, had been deposited on the back surface of the silicon, and served to simulate the heat source. The input voltage and current were controlled by a power supply. The heater was coated with a thin layer of black diffusive paint, with emissivity of $\varepsilon \approx 0.96$. The heater has a serpentine pattern as shown in Fig. 2. The heater filament has a dimension of 0.001 mm in thickness, 0.2 mm in width and 250 mm in length. This design allows a uniform heating of the surface and reduces the contact resistance between the heater and the wafer. To estimate the resistance between the heater and the channel wall the problem has been solved numerically, using The Fluent 5.3 software package. Steady state heat transfer equations were solved

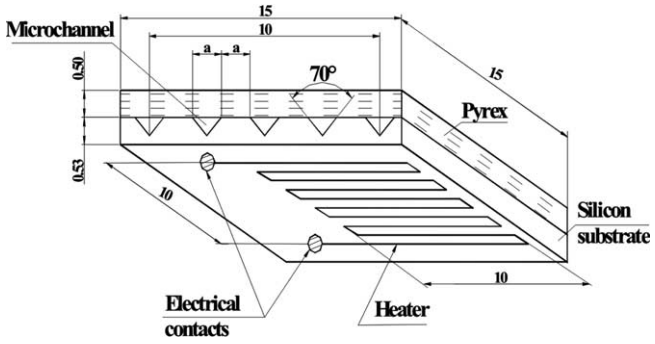

Fig. 2. Test module.

Table 1
Experimental uncertainty

NN	Source of uncertainty	Symbol	Uncertainty, %
1	Hydraulic diameter	d_h	2
2	Heat flux	q	4
3	Mass flux	m	5
4	Vapor quality	x	12
5	Heat transfer coefficient	h	18
6	Reynolds number	Re	9
7	Boiling number	Bo	7

simultaneously in the fluid and in the solid phase. To get the solution the temperature on the inclined surface of the micro-channel should be imposed. This, however, could not be done because it was not known. Instead, the temperature on the channel wall was estimated by an iterative procedure. The given input value of this temperature was assumed. The software made it possible to calculate the temperature on the heater. This temperature was compared to that obtained from experiment. Then the value of the temperature on the channel wall was adjusted up to the difference between the calculated and measured temperature was less than 0.1%. The overall thermal resistance of the silicon substrate and contact thermal resistance of the heater was estimated of 3.6×10^{-6} m^2 K/W (Tiselj et al., 2004). This thermal resistance was used for calculation of the mean temperature at the heated channel wall and the boiling heat transfer coefficient. The difference between the temperature measured at the heater (back of the wafer) and at the wall of the micro-channels was estimated as $\Delta T_1 = 0.3$ K at $q = 80$ kW/m^2 and $\Delta T_2 = 1.2$ K at $q = 330$ kW/m^2. It is included in uncertainty values. The uncertainty of the heat transfer coefficient is given in Table 1.

2.3. Flow and thermal visualization

The flow and thermal visualization technique is shown in Fig. 3. To determine the time of the presence of the liquid phase on the heated wall flow visualization was conducted at constant mass flux $m = 95$ kg/m^2 s in the range of heat flux $q = 80$–330 kW/m^2. A microscope with zoom ability

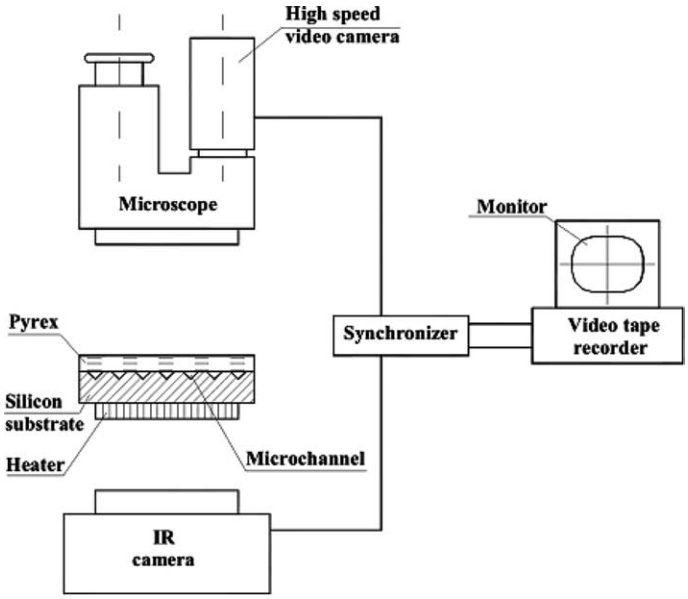

Fig. 3. Flow and thermal visualization.

up to ×40 was connected to an external lighting arrangement. An additional camera joint was assembled to connect a high-speed camera to the microscope. The high-speed camera with maximum frame rate of 10,000 fps, was used to visualize the two-phase flow regimes in the micro-channels.

A thermal imaging radiometer was used to study the temperature field on the electrical heater. Its recording rate was 25 frames per second, with a resolution of 256 pixels per line and typical minimum detectable temperature difference of 0.1 K. The instantaneous field of view was 1.8 mrad. With the radiometer one can obtain a quantitative thermal profile in the point mode, in the line mode (among other things, along the heated wall of the micro-channel), and in the area mode. In the present study, the frequency of the bubble growth in the micro-channel is higher than that of the radiometer, hence we confirmed ourselves to the measurements of temperature field, on the heated bottom of the test module, averaged over a time interval of 0.04 s.

2.4. Procedure

For a normal testing procedure, the pump was turned on and the electrical power to heater was adjusted to a desired level by a voltage controller. The module was then allowed to reach a steady state, which was achieved within 4–5 min from the moment the flow conditions were stabilised. At each test condition, three sets of video images and images of the temperature field on the heater were captured simultaneously. One set of video was near the micro-channel inlet, the second was in the middle, and the third set was near the exit of the micro-channel.

The following procedure was used to determine the wall temperature of the micro-channels from an infrared image of the heater. Positions on the tested wall were determined using the Ther-Monitor image-processing software. They are projections of the channel axes on the back

surface to which the heater is attached. Hence, we have the straight lines on the bottom of the heated module corresponding to the streamwise axes of each micro-channel. Along each line, the temperature on the heated wall was determined. The two-phase data points require detailed analysis. In two-phase flow, the flow began as subcooled single-phase and changed under conditions of the present experiments into explosive two-phase flow. The vapor may be generated only in part of the parallel micro-channels. The location of the saturation temperature is unknown. The simultaneous images obtained from flow and thermal visualization were analyzed to distinguish the part of the parallel micro-channels where boiling occurred. Then the temperature on the heater along each micro-channel was measured and the area available for boiling heat transfer was determined. Fig. 4 illustrates a typical infrared image of the heater obtained at $m = 95$ kg/m^2 s and $q = 160$ kW/m^2. The flow moves from the bottom to the top, the area of the whole heater is 1×1 cm^2 (Area 1 is the hole large square). Area 1 shows the temperature distribution in the streamwise and spanwise directions. The mean temperature on the whole heater was less than the saturation temperature, which indicates that boiling did not occur in the part of this area. There are a hot spots on the Area 1 where the boiling occurred, since $T_{max} = 113.0$ °C. If the mean temperature, was less than saturation temperature it indicates that boiling did not occur in the part of the test module. From Fig. 4 one can see that the mean temperature on the Area 1 is $T_{mean} = 96.1$ °C. There are the following two mechanisms: (i) heating fluid from the inlet temperature to saturation temperature, (ii) single phase fluid flow into certain micro-channels. In the present study we consider part of the whole heater, along which the minimum temperature on the channel wall exceeds the saturation temperature. Area 2 (marked as the small square) shows the temperature distribution in the streamwise and spanwise directions at such part of the heater.

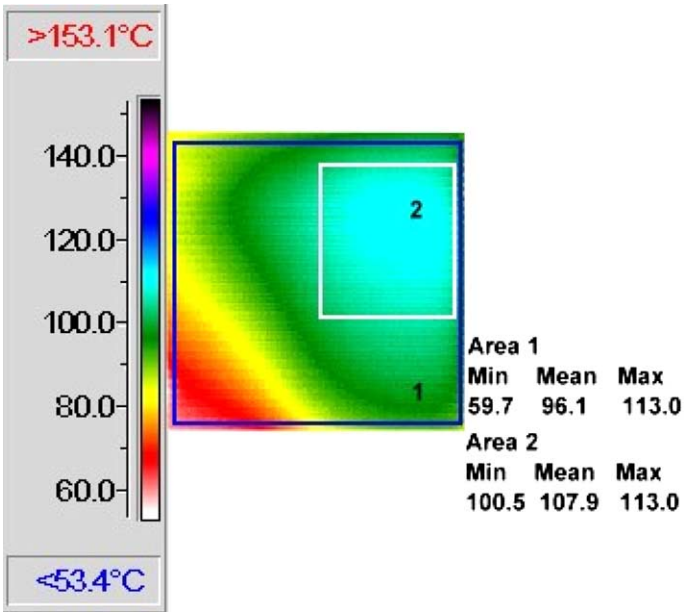

Fig. 4. Thermal field on the heater, $F = 1 \times 1$ cm^2: $m = 95$ kg/m^2 s, $q = 160$ kW/m^2. (1) Area of the whole heater and (2) area of the part of the heater, where saturated flow boiling occurs.

The mean temperature of this area is $T_{mean} = 107.9$ °C, the minimum and maximum temperatures are $T_{min} = 100.5$ °C and $T_{max} = 113.0$ °C. The mean temperature on Area 2 was used for calculating the mean temperature at the heated channel wall and the boiling heat transfer coefficient.

One can see that the temperature field on the heater is non-uniform. The inlet fluid temperature was less than saturation temperature. That leads to significant increase in the temperature on the heater in the streamwise direction. Although the channels were made in such a way that the cross-section of all channels would be uniform, the flow rate through each channel may not be equal. The distribution of flow rate through the channels depends on the way of connection of the test section to the inlet and outlet manifolds. This unevenness leads to non-uniformity of the heater temperature in the spanwise direction.

2.5. Data reduction

The parameters used in the data reduction and analyses are summarized below.

2.5.1. Heat flux

In order to determine the heat flux from the heater to the working fluid, the heat losses due to conduction, convection and radiation were taken into account. There are several heat transfer surface areas that may be used in the calculations. The first is the plate area of the heater $F = 1 \times 1$ cm^2. The second, F_h, can be defined relative to the mean heat flux along the heated perimeter. A comprehensive discussion on the application of these two definitions to evaluate the mean heat flux is presented by Qu and Mudawar (2003). In the present study $F = F_h$, and the heat flux transferred to the fluid was defined as

$$q = \varphi N / F_h \tag{1}$$

where φ is the ratio of the heat transferred to the working fluid to the local heat generation. The total heat balance of the test section may be expressed as

$$N = N_1 + N_2 + N_3 \tag{2}$$

where N is the power generated by Joule heating, N_1 is the power transferred to the fluid, N_2 is the power conducted axially through the silicon wafer, and N_3 is the heat losses.

The power generated by Joule heating was calculated as

$$N = I^2 R \tag{3}$$

The electric resistance of the test section should vary with the outer wall temperature as

$$R = R_0(1 + \mathrm{TCR})(T_w - T_0) \tag{4}$$

where R and R_0 are the values of the resistance at temperature T_w and T_0, respectively, TCR is the temperature coefficient of resistance of the test section. The initial temperature T_0 is taken as 20 °C.

For single-phase flow the power transferred to the fluid moving into the pipe:

$$N_1 = mC_p(T_{f,out} - T_{f,in}) \tag{5}$$

where m is the mass flow rate, C_p is the specific heat, $T_{f,out}$ and $T_{f,in}$ are the fluid temperatures at the outlet and the inlet manifolds.

The heat losses, N_3, from the test section to the environment due to free convection and radiation depend on the outer wall temperature, T_w, and the environmental temperature, T_{air}. They were calculated using equations given in the literature.

The power conducted axially through the silicon wafer was calculated as

$$N_2 = N - N_1 - N_3 \tag{6}$$

For single-phase flow the dependences of N_2 on T_w and N_3 on T_w were obtained and extrapolated to those wall temperatures, T_w, with boiling in the micro-channels. In this case the ratio φ was calculated as

$$\varphi = (N - N_1 - N_2)/N \tag{7}$$

The values φ estimated with standard deviation of 12% were in the range of 0.8–0.9 depending on flow rate and heat flux.

2.5.2. Mass flux

The mass flux, m, at the inlet of test section was calculated as

$$m = Q\rho/A \tag{8}$$

where Q is the volumetric flow rate, ρ is the fluid density, and A is the overall cross-section of the micro-channels.

2.5.3. Reynolds number

$Re = ud_h/v$, where v is the kinematic viscosity calculated at the inlet water temperature, u is the mean flow velocity of the single liquid phase, d_h is the hydraulic diameter.

2.5.4. Heat transfer coefficient

The assumption of thermal equilibrium was used to calculate the heat transfer coefficient in the boiling regime

$$h = q/(T_{w,mean} - T_{s,mean}) \tag{9}$$

where h is the heat transfer coefficient, $T_{w,mean}$ is the average temperature at the channel wall where saturated boiling occurs, $T_{s,mean}$ is the average saturation temperature. The pressure at the inlet and the outlet manifolds was measured, and linear interpolation was employed to determine the saturation temperature.

2.5.5. Mass vapor

Mass vapor quality at the outlet manifold was calculated from equation of change in the enthalpy of a liquid–vapor system during evaporation in the micro-channels.

2.6. Experimental uncertainty

The temperature of the heated wall was measured with an accuracy 0.3 K (95% confidence level). The uncertainty of the components for an estimation of an error measurement of wall temperature was obtained according to the standard 1995 Guide to the Expression of Uncertainty of

the Measurements (GEUM, 1995). The details of calculation are presented by Hetsroni et al. (2003a,b). The error in determining the heat transfer coefficient was calculated from an estimation of the errors that affect the measurement of the following quantities: heat flux and the difference between average value of the average heater temperature and average value of saturated temperature.

The error in determining the power generated by Joule heating is due to errors of measurement of both the electric current and the electric resistance. The error in estimation of the heat losses is due to correlations for calculation of natural convection and radiation heat transfer. The uncertainties in determining various parameters in this study are given in Table 1.

3. Results

3.1. Flow pattern

3.1.1. Flow pattern and heat transfer mechanisms

Two-phase micro-channel heat sinks generally involve flow boiling in straight, constant cross-sectional channels. Flow boiling in parallel channels was studied from the subcooled liquid entry at the inlet to a liquid–vapor mixture flow at the outlet. Once nucleation begins, the heat flux causes a sudden release of energy into the vapor bubble, which grows rapidly and occupies the entire channel. The vapor slug may be considered as an elongated bubble. The rapid bubble growth pushes the liquid–vapor interface on both caps of the vapor slug at the upstream and the downstream ends and leads to a reversed flow. When in some parallel channels the liquid on the upstream side is pushed back, the other parallel channels carry the resulting excess flow. Fig. 5 illustrates two-phase flow, driven by the pump, in a certain part of the parallel micro-channels. It is the top view and the flow pattern was observed through the transparent cover. The field of view is 8 mm in the streamwise direction and 4 mm in the spanwise direction, the flow moves from the bottom to the top, the mass flux is $m = 95$ kg/m^2 s and the heat flux is $q = 160$ kW/m^2. The vapor (the white regions in Fig. 5) may be observed at different distances from the inlet of the micro-channels. The successive images obtained, using high speed video visualization, showed that the flow patterns were periodic. The liquid front was seen to pass periodically the region located near the inlet manifold, the vapor phase occupied most of the channel core, the periodic wetting and rewetting phenomena were also observed. The behavior of the long vapor bubbles occurring in a micro-channel was not similar to annular flow with intermitted slugs of liquid between two long vapor trains. The periodic phenomena described above may be regarded as explosive boiling. The trigger mechanism of such a regime is venting of elongated bubble due to very rapid expansion. Downstream of the ONB point region of the venting of elongated bubble and dryout was observed.

3.1.2. Bubble growth in micro-channel

The location (along the channel) of the appearance of the first bubble at a given flow rate, depends on the local surface temperature variation. Since the heated length of the test section is short (10 mm), at high values of heat flux significant interaction takes place between the steam generated in the micro-channel and the feed water. It is very difficult to capture the behavior

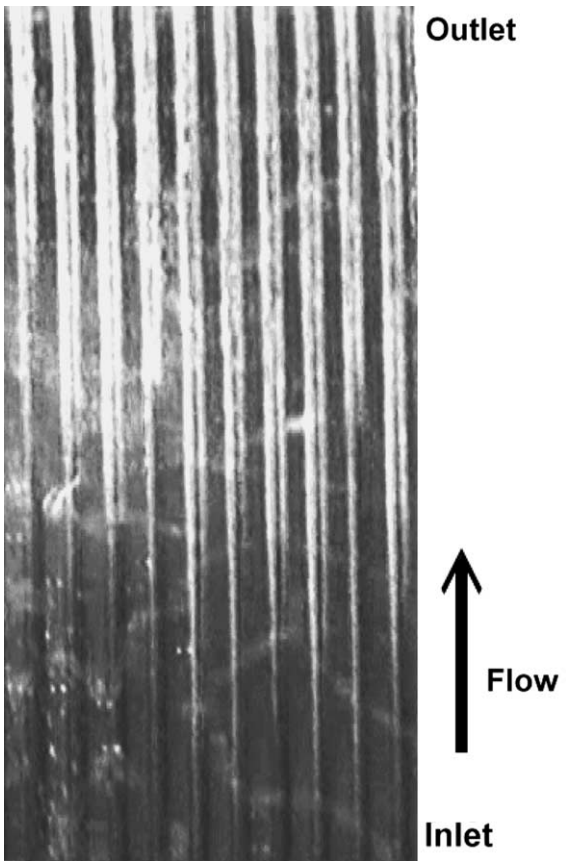

Fig. 5. Flow boiling in parallel micro-channels: $m = 95$ kg/m^2 s, $q = 160$ kW/m^2.

of the elongated bubble at high values of heat flux. We investigated this phenomenon at the mass flux $m = 95$ kg/m^2 s and the heat flux $q = 80$ kW/m^2. Fig. 6a–h show a sequence of bubble formation in one of the parallel triangular channels of $d_h = 129$ μm. The visualization of the flow pattern was realized near the ONB point. The boiling incipience is a local phenomenon, which strongly depends on both the hydrodynamic and thermal conditions. The onset of nucleate boiling (ONB) was established when the first bubbles were observed and the channel wall exceeded the saturation temperature. In general, at given flow rate the ONB location moved upstream as the heat flux increased, as in ordinary sized channels. The main flow moved from the bottom to the top. Fig. 6a shows a single bubble, which begins to grow along the channel. Fig. 6b–d illustrates the bubble growth in the axial direction. Note that at this stage the bubble expands preferentially in the streamwise direction. Fig. 6e–f shows venting of the elongated bubble. Fig. 6g and h show rewetting. The life time of the elongated bubble (the time between images shown in Fig. 6e and b) is about 0.01 s. At a given mass flow rate the life time sharply decreases with increasing heat flux. That is why under certain conditions (periodic flow reversal) we consider the mechanism of saturated boiling in micro-channels as explosive boiling process. Hetsroni et al. (2001, 2002,

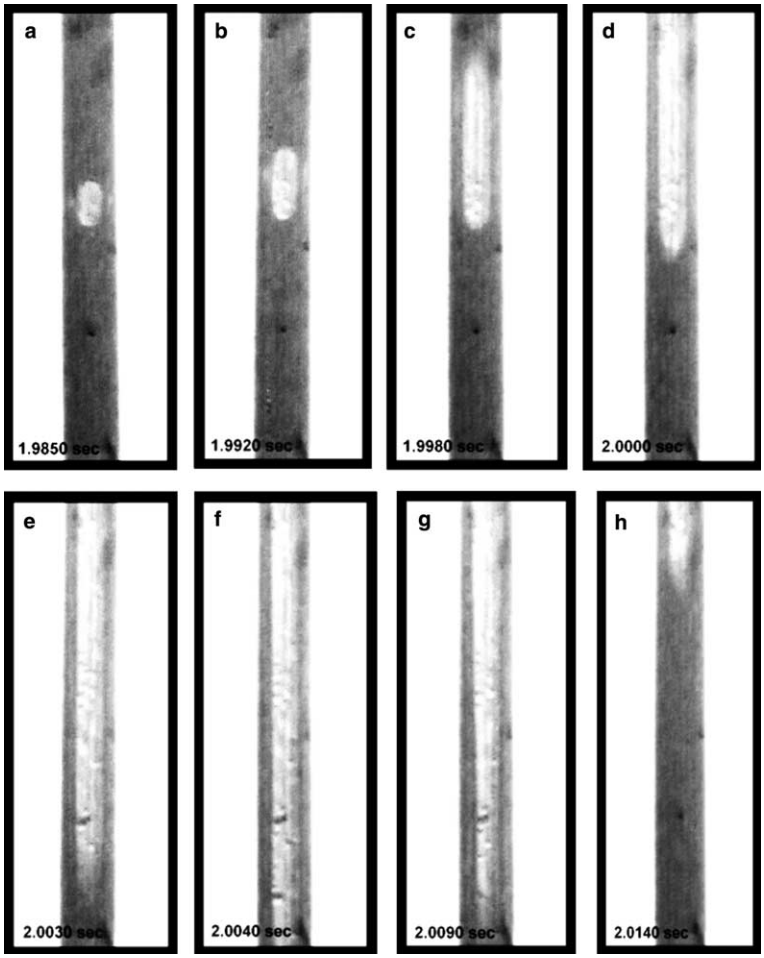

Fig. 6. Bubble growth near outlet manifold: $m = 95$ kg/m^2 s, $q = 80$ kW/m^2.

2003a,b) observed a rapid flow reversal inside an individual channel in parallel triangular micro-channels, Steinke and Kandlikar (2003) reported reverse displacement in a set of six parallel micro-channels, $d_h = 200$ μm. The system departs from stable operating conditions and hydrodynamic instability occurs. This boiling mode leads to liquid–vapor alternating flow in the region located near ONB.

3.1.3. Region along the channel after venting of an elongated bubble

After venting of the elongated bubble, the region of ''liquid droplets'' begins. The vapor phase occupies most of the channel core. The distinct feature of this region is the periodic dryout and wetting phenomenon. The duration of the ''two-phase period'', i.e. the presence of a vapor phase and micro-droplet clusters on the heated wall affects the wall temperature and heat transfer in micro-channels. As the heat flux increases, while other experimental conditions remain unchanged, the duration of the ''two-phase period'' decreases, and CHF is closer.

Fig. 7a–o illustrate a typical example of alternate two-phase flow pattern at a distance of 1000–1500 μm downstream from the inlet of the test section. In Fig. 7a–o a single triangular channel and the walls between the adjacent channels (white strips) are depicted in the central part and in the peripheral parts of each image, respectively. The field of view (including the channel and the walls) is 0.6×0.6 mm, the flow moves from the bottom to the top, the mass flux is $m = 95$

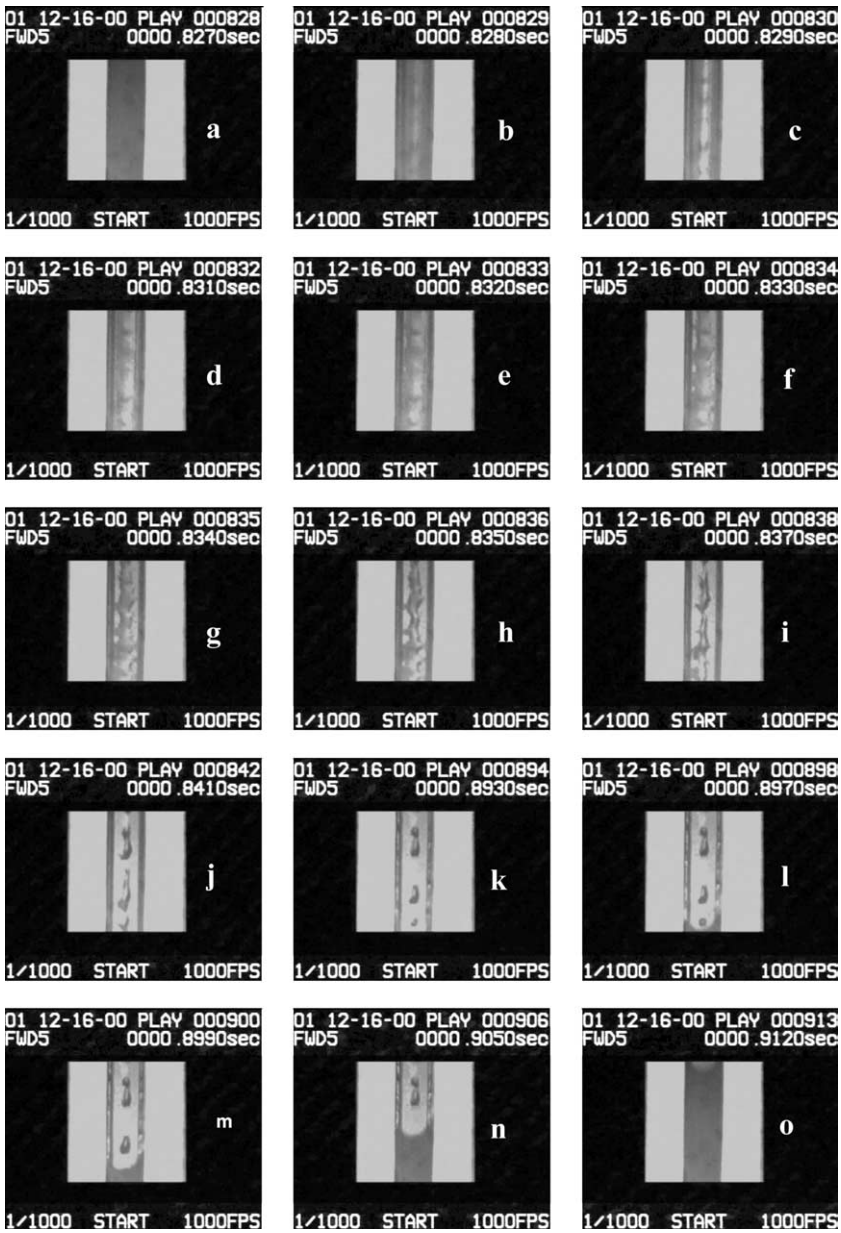

Fig. 7. Flow pattern near inlet manifold: $m = 95$ kg/m^{2}s, $q = 160$ kW/m^2.

kg/m^2 s, the heat flux is $q = 160$ kW/m^2. Fig. 7a shows the water flow that moved through the micro-channel. When the water moves along the channel it is heated up to saturation temperature and then the elongated bubble ventings in a short time. Fig. 7b displays the onset of two-phase reversal flow, which evolved due to venting of the elongated bubble downstream from the observation point. From Fig. 7a and b one can conclude that at the specified conditions of this experiment, the life time of the elongated bubble did not exceed 0.001 s. Comparison between the present results obtained at the mass flux $m = 95$ kg/m^2 s and the heat flux $q = 160$ kW/m^2 to those shown in Fig. 6 and obtained at the mass flux $m = 95$ kg/m^2 s and the heat flux $q = 80$ kW/m^2 reveals that doubling the heat flux, causes an approximately tenfold decrease of the life time of the elongated bubble.

Fig. 7c–f shows the annular flow, where the liquid film on the wall is symmetrically distributed. This flow pattern was also observed by Serizawa et al. (2002) in air–water and in steam–water flow. The authors concluded that there was no essential difference between the two cases (air–water and steam–water flow). In spite of similarity between annular flow in air–water and steam–water flow, our results do not support the conclusions of Serizawa et al. (2002). The authors assumed, when the gas flow rate was sufficiently high in air–water flow in micro-tube, the length of the gas bubble increased, while that of the liquid slug decreased. At a certain gas flow rate, the following gas slug penetrated into the liquid, forming and therefore a liquid ring forms and is observed continuously during long time interval. In the present study annular flow was powered by venting of the elongated bubble and had a short duration (about 0.004 s).

Fig. 7g–h displays the onset of dryout, where liquid droplets are accumulated at the bottom of the triangular channel. Fig. 7i–k shows that the amount of liquid phase decreases, and only few droplets of water remain on the channel bottom. Fig. 7l shows the beginning of wetting and the channel is filled with liquid, Fig. 7m–o. Flow pattern depicted in Fig. 7a–o were also observed by Serizawa et al. (2002) in steam–water flow in a 50 μm silicon tube. The authors reported that at low liquid flow rates, partially continuous liquid film flow changed to the rivulets or even to discrete liquid lumps or large liquid droplets.

The periodic phenomenon described above reveals that the entire channel acts like the area beneath a growing bubble, going through periodic drying and rewetting. The cycle was repetitive with venting of the elongated bubble.

3.2. Flow instability

3.2.1. Pressure drop fluctuations

Occurrence of single-phase liquid flow and two-phase liquid–vapor flow, which appear alternatively with time in the micro-channel, leads to pressure drop fluctuations. The dependence of $(\mathrm{RMS}\Delta P)/\Delta P$ on vapor quality, x, is plotted in Fig. 8 where ΔP is the pressure drop. We did not observe the long period (up to 78 s) pressure and temperature fluctuations reported by Wu and Cheng (2003, 2004). Oscillation amplitudes increase with increasing vapor quality. The flow visualization and the measurements showed that an increase in vapor quality was due to an increase in the heat flux and the time of dryout. The latter leads to a decrease in the heat transfer coefficient. A more detailed explanation of this phenomenon will be presented in the following section.

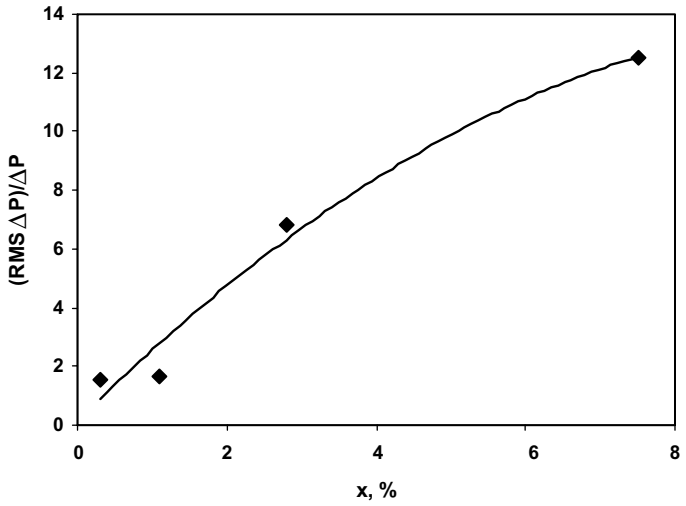

Fig. 8. Dependence of (RMSΔP)/ΔP on vapor quality.

3.3. Physical model

3.3.1. Description of the model

We propose a physical model for the explosive boiling and dryout, based on close inspection of pictures taken by the high-speed video recorder. In order to understand why dryout occurred even at low value of vapor quality, x, it is important to keep in mind that the liquid film does not cover the entire heated surface of the micro-channel, and two-phase flow is characterized by an unsteady cyclic behavior. The following assumptions are made in the development of the model:

1. The bubble nucleation occurs at the location where the wall temperature exceeds the saturation temperature.
2. The heat flux is uniform and constant along the inner wall of the micro-channel.
3. All energy entering the fluid is used to vaporize the liquid. The temperatures of the liquid and vapor remain at saturation temperature.
4. After the bubble venting the liquid remains attached to the wall as droplets or clusters of droplets. It evaporates during the period of the cycle.
5. The thermal inertia of the wall is negligible, i.e. we assumed no phase shift between temperature on the channel wall and the heater.

Fig. 9 shows a representation of the explosive boiling process. The bubble is assumed to nucleate near the ONB point, Fig. 9a. Then the bubble starts quickly to grow to the channel size and an elongated bubble is formed. During this process some amount of liquid remains in front of the bubble, Fig. 9b. Fig. 9c shows bubble venting. During this process the bubble expands not only in the upstream but also in the downstream direction. An interesting result is that a single bubble cyclically growing and collapsing away from the outlet manifold is capable of inducing a mean unidirectional fluid flow. This trend was also reported by Ory et al. (2000). Fig. 9d shows the

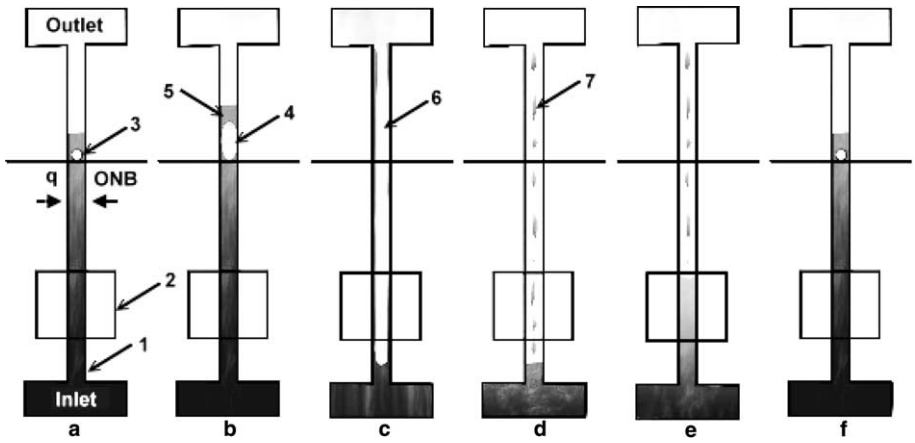

Fig. 9. Scheme of explosive boiling: (1) micro-channel; (2) area of visual observation; (3) ONB point; (4) elongated cylindrical bubble; (5) liquid in front of the bubble; (6) vapor; (7) liquid droplets and clusters.

appearance of liquid droplets or clusters of liquid droplets on the wall after the bubble venting. The pressure in the micro-channel decreases and water starts to move into it from the inlet manifold, Fig 9e. Fig. 9f shows the start of a new cycle.

3.3.2. Period between successive cycles

As described in Section 3.1, the flow pattern was recorded through the observation window located close to the inlet manifold. Fig. 10 illustrates a cyclic variation of events during explosive boiling. The time intervals shown in this figure are: t_1—time for bubble growth from nucleation to channel size, t_2—time of growth elongated bubble up to venting, t_3—time of presence vapor and liquid droplets on the wall, t_4—time of presence single liquid flow downstream ONB. The time interval between cycles, t, was determined as the time between appearance of single liquid flow downstream ONB. It should be stressed that upstream of ONB (i.e. in the saturated boiling

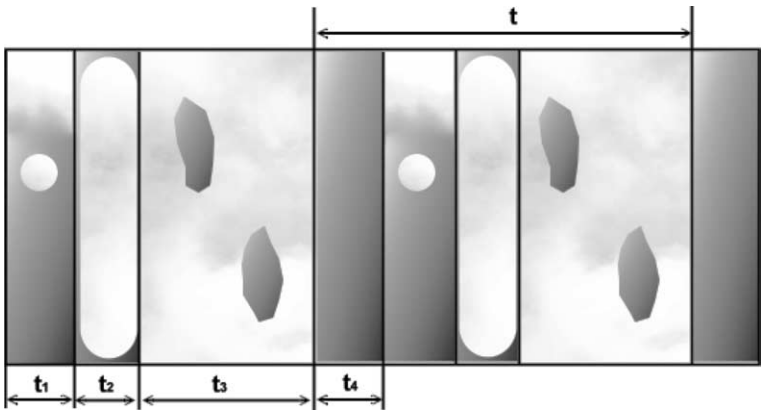

Fig. 10. Cyclic variation of events during explosive boiling.

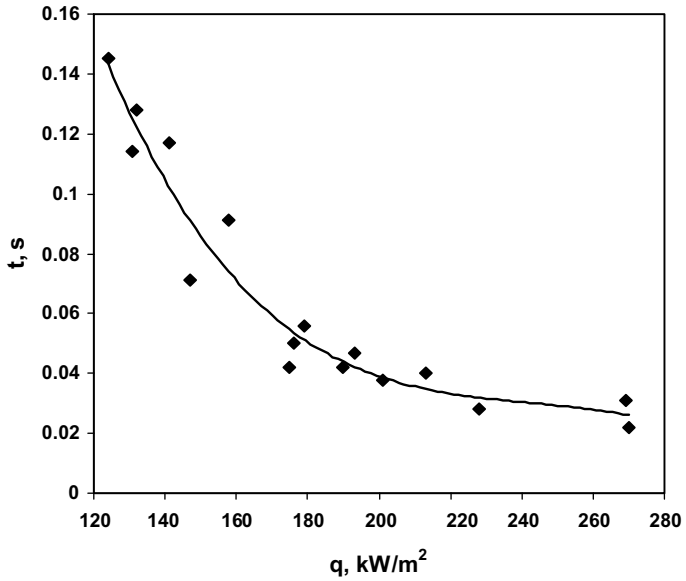

Fig. 11. Dependence of time interval between cycles on heat flux.

region) dryout takes place during the whole period t. Due to the unsteady character of the boiling process, the time interval between cycles is described in statistical terms. For each regime the time period was obtained using histograms of statistical distribution. Fig. 11 shows the dependence of the time interval between cycles, t, on the heat flux, q, at constant value of mass flux $m = 95$ kg/m^2 s. It is seen from Fig. 11 that increasing the heat flux about twofold leads to increasing the cycles of dryout about sevenfold.

3.3.3. The average thickness of the liquid film

The evaporation of the liquid layer on the wall was used by Qu and Mudawar (2003) and Thome et al. (2004) to predict the heat transfer coefficient. In the present study the term "initial liquid film thickness" is used as the average thickness of liquid, distributed during a period t, over the surface of a circular micro-channel after venting of the elongated bubble. This surface is located upstream of the ONB and may be characterized by the heated length L and hydraulic diameter d_h. We assumed that during the period, t, the liquid film has disappeared due to evaporation. The heat removed from the surface of the wall is the same as required for the liquid film evaporation during period, t. The heat balance is

$$\pi d_h L \rho_L = q \pi d_h L t / h_{LG} \tag{10}$$

where ρ_L is the liquid density, h_{LG} is the latent heat of evaporation.

The average liquid thickness, δ, can be calculated as

$$\delta = qt/\rho_L h_{LG} \tag{11}$$

Fig. 12 shows the dependence of the average liquid thickness, δ, on the heat flux, q. In the range of $q = 120$–270 kW/m^2 and $m = 95$ kg/m^2 s the film thickness decreases from 8 μm to 2 μm with increasing heat flux. The maximum and minimum film thickness measured by Moriyama and In-

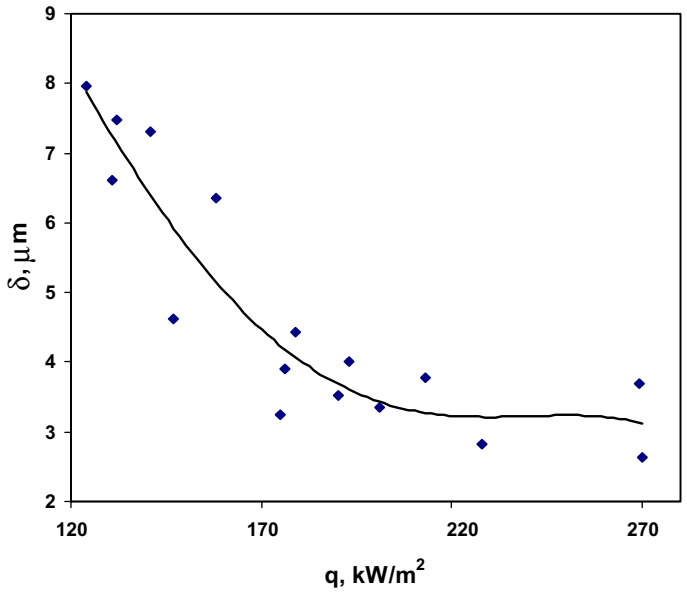

Fig. 12. Dependence of average liquid film thickness on heat flux.

oue (1996) are 7 μm and 2 μm, respectively. The variation of film thickness in the range of $q = 630$–290 kW/m^2 and $m = 255$ kg/m^2 s calculated by Qu and Mudawar (2003a) is in the range of 10–20 μm. Eq. (6) was used to estimate the initial thickness of the thin liquid layer that was formed on the wall of a circular channel of a diameter equivalent to the hydraulic diameter of the triangular channels used in the present study. The heat flux was assumed uniform and the effect of surface tension, that may gather liquid in the corners, was not taken into account. Our results do not differ significantly from those reported in the literature. The simple model used in the present study predicts qualitatively well the dependence of liquid film thickness on heat flux. Decreasing liquid film thickness with increasing heat flux is a distinct feature of dryout during explosive boiling. The time, which the heated surface, located upstream of the ONB, is covered by liquid decreases with an increase of the heat flux, the average film thickness decreases and the heat transfer coefficient decreases as well.

3.4. Heat transfer

Fig. 13 shows dependence of the saturated flow boiling heat transfer coefficient, h, on the thermodynamic equilibrium quality, x, at the outlet collector of the test section. The data were obtained in the range of mass flux from 95 to 340 kg/m^2 s. As indicated in Fig. 13, h decreases appreciably with increasing x. This trend agrees with results reported by Qu and Mudawar (2003), Kandlikar (2004) and Kandlikar and Balasubramanian (2004). The overall range of $h = 10$–30 kW/m^2 K is fairly similar to that measured by Qu and Mudawar (2003), $h = 20$–45 kW/m^2 K, and by Yu et al. (2002), $h = 10$–50 kW/m^2 K (the latter is for water flow boiling in a single mini-tube).

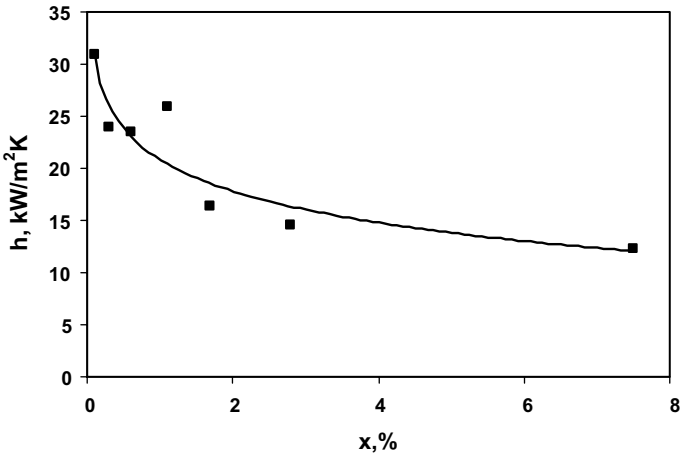

Fig. 13. Dependence of heat transfer coefficient on vapor quality.

The results presented in Fig. 13 show that the heat transfer coefficient does not depend on the mass flux. These results are in contradiction with those reported by Qu and Mudawar (2003). The authors pointed to annular flow as the dominant two-phase flow pattern in micro-channel at $Re = 60$–300 and concluded that the saturated flow boiling heat transfer coefficient is a strong function of the mass flux and only a weak function of the heat flux. They suggest that the dominant heat transfer mechanism for water micro-channels heat sinks is forced convective boiling. Flow visualization results of the present study show that when the Reynolds number is smaller, the explosive boiling region occurs.

Moriyama and Inoue (1996) and Ory et al. (2000) studied the growth and venting of a vapor bubble in a narrow space. The role of the peak velocity, V, (peak velocity of the vapor front) was discussed. In terms of this peak velocity, V, the Reynolds and the Weber numbers are defined in the usual way by

$$Re = Vd/v, \quad We = d\rho V^2/\sigma \tag{12}$$

Here ρ, v, and σ are the density, viscosity, and surface tension coefficients of the liquid, d is the characteristic diameter. The main difficulty in the use of the Reynolds and Weber numbers is in estimating the peak velocity of the vapor front. Ory et al. (2000) suggest as characteristic dimensionless time of the process dimensionless quantity

$$Z = Re/We^{0.5} = (d^2/v) \times (\sigma/\rho d^3)^{0.5} \tag{13}$$

This quantity, which equals the inverse Ohnesorge number, $Oh = \mu/(\rho d\sigma)^{0.5}$, may be interpreted as the ratio of the viscous force to the square root of the product of the inertia and the surface tension forces. It should be noted that explosive boiling could not be clearly attributed to any single non-dimensional number.

To fully understand the heat transfer phenomenon, the effect of the heat flux on the heat transfer coefficient should be addressed. The observed trend of decreasing h with increasing x implies heat transfer coefficient may also decrease with increasing heat flux. Hetsroni et al. (2002) demonstrated that both these mechanisms occurred during saturated flow boiling of Vertrel XF in

micro-channels. A decrease of heat transfer coefficient with increasing heat flux does not support the nucleate boiling mechanism observed in channels of $d_h > 3$ mm, which is normally associated with a significant increase in h with increasing q (Collier and Thome, 1994).

4. Conclusions

Flow visualization showed that the behavior of long vapor bubbles occurring in a micro-channel at low Reynolds numbers is not similar to annular flow with intermittent slugs. This process may be described as explosive boiling with periodic wetting and dryout.

Occurrence of single-phase liquid flow and two-phase liquid–vapor flow, which appears alternately in the micro-channel, leads to pressure drop fluctuations. The amplitudes of pressure drop fluctuations increase with increasing vapor quality.

This study shows strong dependence of the heat transfer coefficient on vapor quality. The time of the presence of liquid on the heated surface decreases with increasing heat flux. Dryout occurs immediately after venting of elongated bubble.

This study proves that under certain flow and heat transfer conditions explosive boiling occurs in micro-channels. It should be stressed that the bubble behavior and heat transfer were studied only for water flow in triangular channels of a given size. The new experiments should be conducted to apply these results to other situations and to obtain non dimensional numbers that could describe explosive boiling.

Acknowledgments

This research was supported by the Fund for Promotion of Research at the Technion. A. Mosayk is supported by a joint grant from the Center for Absorption in Science of the Ministry of Immigrant Absorption and the Committee for Planning and Budgeting of the Council for Higher Education under the framework of the Kamea Program, and E. Pogrebnyak was supported by the Center for Absorption in Science, Ministry of Immigrant Absorption State of Israel.

References

Collier, J.G., Thome, J., 1994. Convective Boiling and Condensation, third ed. Oxford University Press.

Dupont, V., Thome, J.R., Jacobi, A.M., 2004. Heat transfer model for evaporation in micro-channels, Part II: Comparison with the database. Int. J. Heat Mass Transfer 47, 3387–3401.

Guide to the Expression of Uncertainty of Measurement, Geneva, International Organization for Standardization, 1995.

Hetsroni, G., Mosyak, A., Segal, Z., 2001. IEEE Trans. Comput. Packaging Technol. 24, 16–23.

Hetsroni, G., Mosyak, A., Segal, Z., Pogrebnyak, E., 2003a. Two-phase flow patterns in parallel micro-channels. Int. J. Multiphase Flow 29, 341–360.

Hetsroni, G., Gurevich, M., Mosyak, A., Rozenblit, R., 2003b. Surface temperature measurement of a heated capillary tube by means of an infrared technique. Measur. Sci. Technol. 14, 807–814.

Hetsroni, G., Mosyak, A., Segal, Z., Ziskind, G., 2002. A uniform temperature heat sink for cooling of electronic devices. Int. J. Heat Mass Transfer 45, 3275–3286.

Jiang, L., Wong, M., Zohar, Y., 2001. Forced convection boiling in a micro-channels heat sink. J. Microelectromech. Syst. 10, 12–17.

Kandlikar, S.G., 1990. General correlation for two-phase flow boiling heat transfer coefficient inside horizontal and vertical tubes. J. Heat Transfer 102, 219–228.

Kandlikar, S.G., 2002. Fundamental issues related to flow boiling in mini-channels and micro-channels. Exp. Thermal Fluid Sci. 26, 389–407.

Kandlikar, S.G., Bulut, M., 2003. An experimental investigation on flow boiling of ethylene-glycol/water mixtures. ASME J. Heat Transfer 125, 317–325.

Kandlikar, S.G., Balasubramanian, P., 2004. An extension of the flow boiling correlation to transition, laminar, and deep laminar flows in mini-channels and micro-channels. Heat Transfer Eng. 25, 86–93.

Kandlikar, S.G, 2004. Heat transfer mechanisms during flow boiling in micro-channels. J. Heat Transfer, Trans. ASME 126, 8–16.

McAdams, W.H., Minden, C.S., Carl, R., Picornell, D.M., Dew, J.E., 1949. Heat transfer at rates to water with surface boiling. Ind. Eng. Chem. 41, 1945–1963.

Mehendale, S.S., Jacobi, A.M., Shah, R.K., 2000. Fluid flow and heat transfer at micro- and meso-scales with applications to heat exchanger design. Appl. Mech. Rev. 53, 175–193.

Moriyama, K., Inoue, A., 1996. Thickness of the liquid film formed by a growing bubble in a narrow gap between two horizontal plates. J. Heat Transfer, Trans. ASME 118, 132–139.

Ory, E., Yuan, H., Prosperetti, A., Popinet, S., Zaleski, S., 2000. Growth and collapse of vapor bubble in a narrow tube. Phys. Fluids 12, 1268–1277.

Qu, W., Mudawar, I., 2003. Flow boiling heat transfer in two-phase micro-channel heat sinks—1. Experimental investigation and assessment of correlation methods. Int. J. Heat Mass Transfer 46, 2755–2771.

Qu, W., Mudawar, I., 2003a. Flow boiling heat transfer in two-phase micro-channel heat sinks—2. Annular two-phase flow model. Int. J. Heat Mass Transfer 46, 2773–2784.

Qu, W., Mudawar, I., 2003b. Flow boiling heat transfer in two-phase micro-channel heat sinks—2. Annular two-phase flow model. Int. J. Heat Mass Transfer 46, 2773–2784.

Rohsenow, W.M., Hartnett, J.P., Ganic, E.N., 1985. Boiling, Handbook of Heat transfer Fundamentals, p. 12 (Chapter 12).

Serizawa, A., Feng, Z., Kawara, Z., 2002. Two-phase flow in micro-channels. Exp. Thermal Fluid Sci. 26, 703–714.

Steinke, M.E., Kandlikar, S.G., 2003. Flow boiling and pressure drop in parallel micro-channels. First International Conference on Micro-channels and Mini-channels. ASME, NY, pp. 567–579.

Steinke, M.E., Kandlikar, S.G., 2004. Control and effect of dissolved air in water during flow boiling in micro-channels. Int. J. Heat Mass Transfer 47, 1925–1935.

Thome, J.R., Dupont, V., Jacobi, A.M., 2004. Heat transfer model for evaporation in micro-channels, Part I: Comparison with the database. Int. J. Heat Mass Transfer 47, 3375–3385.

Tiselj, I., Hetsroni, G., Mavko, B., Mosyak, A., Pogrebnyak, E., Segal, Z., 2004. Effect of axial conduction on the heat transfer in micro-channels. Int. J. Heat Mass Transfer 47, 2251–2265.

Wu, H.Y., Cheng, P., 2003. Visualization and measurements of periodic boiling in silicon micro-channels. Int. J. Heat Mass Transfer 46, 2603–2614.

Wu, H.Y., Cheng, P., 2004. Boiling instability in parallel silicon micro-channels at different heat flux. Int. J. Heat Mass Transfer 47, 3631–3641.

Yen, T.H., Kasagi, N., Suzuki, Y., 2003. Forced convective boiling heat transfer in micro-tubes at low mass and heat fluxes. Int. J. Multiphase Flow 29, 1771–1792.

Yu, W., France, D.M., Wambsganss, M.W., Hull, J.R., 2002. Two-phase pressure drop, boiling heat transfer, and critical heat flux to water in a small-diameter horizontal tube. Int. J. Multiphase Flow 28, 927–941.

Zhang, L., Koo, J., Jiang, L., Asheghi, M., Goodson, K.E., Santiago, J.K., 2002. Measurements and modeling of two-phase flow in micro-channels with nearly constant heat flux boundary conditions. J. Microelectromech. Syst. 11, 12–19.